AD695562

TECHNICAL REPORT

MEASUREMENTS OF INCIDENT-SHOCK TEST TIME AND REFLECTED SHOCK PRESSURE AT FULLY TURBULENT BOUNDARY-LAYER TEST CONDITIONS

BY ROBERT G. FUEHRER

CAL No. AN-2514-Y-1

Research Supported By:

THE CORNELL AERONAUTICAL LABORATORY, INC.
WORK AUTHORIZATION: 86-208

SEPTEMBER 1969

CORNELL AERONAUTICAL LABORATORY, INC.
OF CORNELL UNIVERSITY, BUFFALO, N. Y. 14221

Reproduced by the
CLEARINGHOUSE
for Federal Scientific & Technical
Information Springfield Va. 22151

CORNELL AERONAUTICAL LABORATORY, INC.
BUFFALO, NEW YORK 14221

MEASUREMENTS OF INCIDENT-SHOCK TEST TIME AND REFLECTED SHOCK PRESSURE AT FULLY TURBULENT BOUNDARY-LAYER TEST CONDITIONS

CAL TECHNICAL REPORT NO. AN-2514-Y-1

SEPTEMBER 1969

RESEARCH SUPPORTED BY:
THE CORNELL AERONAUTICAL LABORATORY, INC.
WORK AUTHORIZATION: 86-208

Prepared by: R. G. Fuehrer
ROBERT G. FUEHRER

Approved by: J. F. Martin
JAMES F. MARTIN, HEAD
HYPERSONIC FACILITIES DEPARTMENT

DDC
RECEIVED
OCT 31 1969
B

FOREWORD

The work described in this report was supported by Cornell Aeronautical Laboratory internal research funds under cost order 86-208.

This report originates from a paper presented at the Seventh International Shock Tube Symposium held in Toronto, Canada, June 23-25, 1969. The Proceedings of this meeting are not available as of this reporting date (September 1969) but they will be published by the University of Toronto Press some time in the future.

The author wishes to acknowledge W. Lorich and R. Kryszak for their assistance in carrying out the experimental program. Thanks are also due to Dr. J. K. Dukowicz and Dr. M. G. Dunn with whom many informative discussions were held during the course of this work.

ABSTRACT

An experimental study has been made of incident-shock test time and end-wall, reflected-shock pressure at test conditions characteristic of high-pressure, high-enthalpy shock tunnels operating in the tailored-interface mode. The driven gas in these experiments was either air or nitrogen and the driver gas was heated hydrogen. The incident-shock Mach number varied from 7.5 to 10.6 and the initial driven-tube pressure varied from 10 to 150 cm Hg. Measurements of the radiation intensity behind the incident shock and Flagg's interpretation of the end-wall "pressure dip" were used to infer the arrival of the interface region at three different axial stations in the driven tube. Incident-shock test time, for both air and nitrogen, was found to be considerably less than Mirels' turbulent boundary-layer test-time theory predicts at the test conditions commonly used in high-pressure shock-tunnel work. Combustion between the driver and driven gas was observed for the combination of hydrogen and air but this had no measurable effect on the usable test time. Mirels' theory appears to underestimate the mass flow in the boundary layer, particularly at high Reynolds number test conditions. Suitable modifications of this theory are suggested.

TABLE OF CONTENTS

Section		Page
	FOREWORD	i
	ABSTRACT	ii
1.	INTRODUCTION	1
2.	EXPERIMENTAL APPARATUS AND TECHNIQUES	2
	2.1 Test Facility	2
	2.2 Instrumentation	3
	2.2.1 Radiation	3
	2.2.2 Pressure	3
	2.2.3 Shock Velocity	4
	2.2.4 Side-Wall Temperature	4
3.	DISCUSSION OF RESULTS	6
	3.1 Incident-Shock Radiation Measurements	7
	3.2 Side-Wall Temperature Measurements	8
	3.3 End-Wall Pressure Measurements	9
	3.4 Data Analysis	10
4.	CONCLUSIONS	16
	REFERENCES	18
	FIGURES	

1. INTRODUCTION

Over the past several years it has been a common practice to interpret data and predict the performance of high-pressure shock tunnels in terms of driven-gas slug lengths computed from Mirels' turbulent boundary-layer, incident-shock test-time theory[1]. The importance of taking into account wall boundary layer effects in estimating driven-gas slug lengths and incident-shock test time has long been recognized. Laminar boundary-layer theories (e.g. Refs. 2-8) developed for this purpose have generally been in good agreement with experimental data reported by many researchers (e.g. Refs. 5-17). However, Mirels' turbulent boundary-layer theory has never been similarly verified despite its frequent use. A limited amount of turbulent boundary-layer test-time data have been reported [14-18] but these data were obtained either at low incident-shock Mach numbers (i.e. $M_s \leq 5$) [15-18] or at transitional rather than fully turbulent boundary-layer test conditions [14-17]. Data on incident shock test time, at test conditions where present day high-pressure shock tunnels routinely operate, are virtually nonexistent in the open literature.* The experimental investigation described in this report was undertaken therefore to obtain new data on incident-shock test time for fully turbulent boundary-layer test conditions at relatively high shock Mach numbers ($7.5 \leq M_s \leq 10.6$) in air and nitrogen.

*This report is essentially a reprint of the paper presented at the Seventh International Shock Tube Symposium held in Toronto, Canada, June 23-25, 1969. Since this paper was written, additional data have been reported [29], that serves to complement the data presented herein.

2. EXPERIMENTAL APPARATUS AND TECHNIQUES

2.1 Test Facility

The Cornell Aeronautical Laboratory's 96-inch Hypersonic Shock Tunnel (HST) test facility was used to obtain the data presented in this report. The shock tube portion of this facility, depicted in Fig. 1, is a chambered configuration having a 5-inch ID driver and a 4-inch ID, 48.44 ft. long driven tube. The driver is externally heated and operated at a gas temperature of 775F and pressures up to 30,000 psia. Hydrogen was used as the driver gas in these experiments. The theoretical tailoring shock Mach number, corresponding to these driver conditions is 10.3 when air, at an initial pressure of 1 atm., is used for the driven gas. However, because of shock attenuation and other nonideal shock tube effects, the actual "tailoring" shock Mach number for this facility is in the range of 8.0 to 8.5 depending on the driver pressure level.* The data presented in this report were obtained at near-tailored and over-tailored test conditions.

Diaphragm rupture was initiated by means of the double-diaphragm, firing cavity technique, shown in Fig. 1, to obtain reproducible test conditions. The firing cavity was vented to initiate diaphragm rupture so that the upstream diaphragm would always rupture first. This procedure is necessary to avoid the problem of multiple shocks in the driven tube which occur when the firing cavity is pressurized and the downstream diaphragm ruptures a finite time before the upstream diaphragm.

The nozzle throat configuration and centerbody valve (e.g. Ref. 18) normally used in the operation of the CAL 96-inch HST were not used in these tests. The end of the driven tube containing these components was replaced by an instrumented, constant-area tube section (4" ID) terminated by a flat end-plate.

---

*The "tailoring" shock Mach determined experimentally corresponds to the shock Mach number for which the end-wall pressure has an average constant level prior to the arrival of the reflected head of the driver expansion fan. If the average pressure tends to increase with time this test condition would be referred to as being over-tailored.

2.2 Instrumentation

The data presented in this report were obtained from side-wall measurements of the radiation intensity behind the incident shock at station 5 and 7-1/2 (see Fig. 1) and end-wall measurements of the pressure behind the reflected shock. In addition, side-wall measurements of the surface temperature behind the incident shock were obtained at station 10 using a thin-film heat transfer gage to provide data on boundary-layer transition.*

2.2.1 Radiation

The incident-shock test time, determined by the radiation intensity behind the incident shock, was measured with an EG & G Model SGD-100 silicon diffused photodiode, sensitive in the spectral range from 0.5 to 1.05 microns.** The photodiode viewed the radiating gas through a 6-inch long, 1/16-inch ID orifice to assure good spatial resolution. Fused quartz windows (1/8-inch thick) mounted flush with the driven tube ID terminated the orifice of this optical viewport. No optical filtering was attempted in these experiments nor was any effort made to identify the radiating species.

The quartz windows were replaced after every run to eliminate the possibility of window degradation affecting the shape or level of the radiation record. In addition, the bore of the driven tube was thoroughly cleaned before every run with a cloth dampened with acetone in an effort to reduce the level of radiation caused by gas contamination.

2.2.2 Pressure

A Kistler 603H pressure transducer was used for measuring the end-wall reflected-shock pressure. The output of this transducer was filtered

*The term "side-wall temperature" used throughout the report refers to the surface temperature of the substrate of a thin-film heat transfer gage mounted flush with the shock-tube wall.

**Optical transmission in this range is 50% or greater. In the spectral range from 0.35 to 1.13 micron (i.e. from the near ultraviolet to the near infrared) the transmission is 10% or greater. Peak sensitivity occurs at about 0.9 microns.

by means of a specially designed "notch" filter having a 3 dB point at 20 KHz, 37 dB maximum attenuation at 54 KHz and over 20 dB attenuation for all frequencies above 100 KHz. A thin coating (.025-inch thick) of G.E. RTV-102 was applied to the diaphragm of the transducer before every run to provide thermal insulation for the transducer.

2.2.3 Shock Velocity

Incident-shock velocity and trajectory was measured by means of five conventional ionization gages located at stations 4, 6, 7, 8, and 12 in the driven tube (see Fig. 1). High frequency electronic counters were used to record the elapsed time for passage of the shock wave between these stations (i.e. sta. 4 to 6, 6 to 7, etc.). The shock Mach number at the instrumentation stations 5 and 7-1/2 were computed directly from the elapsed time measurements obtained between stations 4 to 6 and 7 to 8, respectively. The end-wall Mach number was determined by linear extrapolation of the shock Mach number attenuation curve constructed for each run. Typical shock attenuation characteristics for the shock tube used in these experiments are given in Fig. 2. The speed of sound used to calculate the shock Mach number was based on measured values of the initial gas temperature and the transport properties given in Ref. 19.

2.2.4 Side-Wall Temperature

Standard thin-film platinum resistance-thermometer gages of the type described by Vidal [20] several years ago were used to measure the side-wall temperature behind the incident shock. Boundary-layer transition time, τ_{tr}, representing the period that the wall boundary layer is laminar at a given station, was determined from these temperature records using the procedure described by Hartunian, et al. [21] Data on τ_{tr} were of interest in establishing the extent to which the test conditions of these experiments satisfied the basic requirement in Mirels' theory that the boundary layer behind the incident shock be fully turbulent.

Considerable care was taken to assure that the response time of the wall-temperature instrumentation was adequate to measure the 1 to 10 μsec transition times anticipated for these test conditions. The thermal

response of various film-substrate combinations were examined using Kurzrock's [22] heat conduction analysis. This led to the selection of a platinum film on a substrate of vitreous alumina (Al_2O_3) for the high initial-pressure test condition (i. e. P_1 = 10 psia) and platinum on Pyrex #7740 for the low-pressure test condition of P_1 = 10 cm. Hg. Initially, no attempt was made to electrically insulate the platinum film from the ionized gas behind the incident shock because this would reduce the frequence response of the gage. Furthermore, some reduction in the laminar temperature step due to electrical shorting of the gage could be tolerated since heat flux measurements were not of interest. No problem was encountered with the noninsulated gages at the P_1 = 10 psia test condition. However at the P_1 = 10 cm. Hg. condition, severe electrical shorting of the film element was experienced. A thin coating of magnesium flouride ($\approx$0. 1 micron thick) had to be applied to the platinum film before data on T_e could be obtained at this test condition.

The output of the thin film gage was recorded on a Tektronix type 545 oscilloscope using a type M preamplifier plug-in unit to maintain the high frequency response capabilities of the entire system. With these precautions, signal rise times of 0. 3 μ sec were achieved with the uncoated alumina gage. This is the best that could be expected since the time for the incident shock to cross the width of the platinum film is about 0. 3 μ sec for the conditions of these tests.

3. DISCUSSION OF RESULTS

Data on incident-shock test time were obtained in air and nitrogen for shock Mach numbers ranging from 7.5 to 10.6 and initial driven tube pressures ranging from 10 to 150 cm. Hg. The driver pressures varied from 1900 to 26,800 psi for the heated hydrogen driver used in these tests.

The primary source of data on incident-shock test time in this program was the side-wall measurements of the radiation intensity behind the incident shock obtained at station 5 and 7-1/2. However, the end-wall reflected-shock pressure proved to be an additional source of information regarding the location of the interface region near the end of the driven tube and also served to corroborate the radiation test time data. These features are illustrated in Fig. 3 which shows typical oscillograms of the incident-shock radiation at stations 5 and 7-1/2 and the end-wall reflected-shock pressure as well as a wave diagram constructed from these data. The oscillograms shown are for hydrogen driving air at an initial pressure of 10 psia. The incident shock Mach number at station 7-1/2 is 8.17. The arrival of the interface region at station 5 is readily determined from the abrupt drop in radiation intensity seen in the radiation oscillogram (Fig. 3a) at a time interval "A" after arrival of the incident shock. The radiation record at station 7-1/2 (Fig. 3b) is similar to station 5 except that an additional source of significant radiation passes the viewing station shortly after the radiation intensity begins to decrease from an established plateau (i.e. after time interval "B"). This latter portion of the radiation record is the result of combustion between the driver and driven gas as a subsequent figure will clearly demonstrate. The "notch" in the radiation record of Fig. 3b, which occurs at the time interval "B" after passage of the incident shock, is a characteristic feature of the radiation records obtained at station 7-1/2 for all test conditions involving hydrogen driving air used in this program. The arrival of the interface region at this station is considered to occur at the beginning of this radiation "notch".

The end-wall reflected-shock pressure of Fig. 3c corroborates the interpretation of the radiation records by the following reasoning. Shortly

after reflection of the incident-shock from the end wall (i.e. at time interval "C") a sudden and significant drop in pressure is seen to occur in the pressure record of Fig. 3c. This easily recognized and very repeatable phenomenon, commonly referred to as the "pressure dip," is well known to operators of hydrogen-driven reflected shock-tunnels. Flagg [23], several years ago, correctly attributed this "pressure dip" disturbance to the interaction of the reflected shock with the combustion region behind the incident shock. Using this interpretation, the time interval "C" (Fig. 3c) represents the time for the reflected shock to encounter the combustion region and return an expansion wave to the end-wall. The location of the interface region near the end of the driven tube can therefore be determined from the "pressure dip" time interval "C", hereafter referred to as Δt "dip", and the theoretical reflected shock velocity and speed of sound (e.g. Ref. 24) by the method shown in the wave diagram of Fig. 3. The interface region located from the end-wall pressure data in this fashion is seen to be in good agreement with the radiation data identified as point "A" and "B" on the wave diagram. The interface region as determined by Mirels' theory[1] is also shown on the wave diagram for comparison. Incident-shock test time for this test condition is seen to be about 2/3 to 1/2 of that predicted by Mirels' theory. The results obtained for other test conditions are discussed in the next three sections.

3.1 Incident-Shock Radiation Measurements

To determine if combustion between the driver and driven gas is responsible for the poor agreement of the experimental data with Mirels' theory the test condition of Fig. 3 was repeated using nitrogen as the driven gas. The resulting nitrogen radiation data obtained at stations 5 and 7-1/2 are given in Fig. 4 along with the corresponding air radiation data for comparison. Incident-shock test time is seen to be essentially the same for nitrogen (Fig. 4a, b) as it is for air (Fig. 4c, d). Thus, although a combustion region definitely exists behind the incident shock (compare Fig. 4b to 4d) and even grows in intensity as it progresses down the driven

tube (compare Fig. 4c to 4d), combustion does not contribute to a reduction in incident-shock test time at these test conditions.*

A summary of the incident-shock test time data obtained from the radiation measurements at stations 5 and 7-1/2 is given in Figs. 5 and 6. Theoretical incident-shock test times derived from Mirels' theory[1] are also given in these figures for comparison.** Incident-shock test time for air is seen from Figs. 5 and 6 to be essentially the same as nitrogen for all the test conditions used in this program. Comparison of these data to Mirels' theory[1] shows that the agreement is poor at high initial pressure levels of the driven gas, P_1, and fair at low values of P_1. In addition, the data exhibit substantially less sensitivity to P_1 than the theory would predict. A possible explanation for these unexpected results is given in the "Data Analysis" section of this report.

3.2 Side-Wall Temperature Measurements

The extent to which the data of Figs. 5 and 6 correspond to fully turbulent boundary-layer test conditions may be determined from Fig. 7 which shows typical oscillograms of wall-temperature records used to obtain boundary-layer transition times, t_{tr}, and from Fig. 8 which gives a summary of boundary-layer transition time data presented in terms of transition Reynolds number. The boundary-layer transition times given in Fig. 7 and in the table of Fig. 8 are seen to be of the order of a few micro-seconds as compared to the incident-shock test times given in Figs. 5 and 6 that are in the range of 120 to 240 μ sec. The laminar boundary-layer portion of the flow behind the incident shock therefore represents less than

---

*It is interesting to note that, for the same initial pressure in the driven tube, the driver pressure required to produce a given value of M_s is about 20% lower when the driven gas is air than it is for N_2 (see Figs. 2, 4). This effect is very repeatable and is probably due to combustion behind the incident shock augmenting the driving energy of the expanding driver gas.

**All theoretical viscous shock-tube parameters given in this report were obtained from a computer program written by the author which is based on the equations given by Mirels in Ref. 1 and the real-gas normal shock properties of Refs. 24, 25. This was necessary because a graphical presentation of the important viscous parameters is not provided for nitrogen in Ref. 1 and that which is provided for air is based on real-gas normal shock properties corresponding to much lower initial-pressure levels than were used in this test program.

3% of the entire incident slug length signifying that the data of Figs. 5 and 6 closely approximate a fully turbulent boundary-layer test condition.

The shock-tube boundary-layer transition data presented in Figs. 7 and 8 were obtained at a unit Reynolds number level that is higher than has ever been reported in the open literature, to the author's knowledge, for high wall-cooling rates (i.e. $M_s \approx 8$). For this reason it was of interest to compare these data, on a transition Reynolds number basis, to the data reported by Hartunian, et al.[21] This result is given in Fig. 8. The agreement with the data of Ref. 21 is fairly good considering that the unit Reynolds numbers involved were 5 to 100 times greater than those of Ref. 21 and that the steel walls of the circular test section used in this test program were substantially rougher than the glass wall rectangular test section used in Ref. 21. It appears, therefore, that reasonable estimates of shock-tube boundary-layer transition times may be obtained for high-pressure shock-tunnel test conditions by using the transition Reynolds number correlation generated by Hartunian, et al.[21] many years ago at comparatively low initial-pressure levels in the driven tube.

3.3 End-Wall Pressure Measurements

In a previous section it was shown that the location of the interface region near the end of the driven tube may be determined from end-wall pressure data (see Fig. 3) when a combustion region exists behind the incident shock by using Flagg's[23] interpretation for the "pressure dip". It is not necessary, however, that the driver and driven gas be combustible in order to establish the location of the interface region in this fashion. From Fig. 9 we see that a "pressure dip" similar to that obtained in air (Fig. 9a) also occurs in nitrogen (Fig. 9b). This is because a region of mixed driver and driven gas always exists behind the incident shock regardless of whether combustion takes place or not. The strength of the disturbance produced when the reflected shock encounters this mixed gas region is, of course, less for nitrogen than for air, as Fig. 9 shows and Dunn[26] working at much lower pressure levels also demonstrated, because combustion produces a greater impedance mismatch. Nevertheless, the "pressure dip"

obtained with nitrogen is sufficiently well defined that inferring the location of the interface region from the nitrogen end-wall pressure data proved to be no more difficult than it was for the air data. A summary of these data expressed in terms of the time interval Δt"dip" (see Fig. 9) is given in Fig. 10 along with the corresponding theoretical time for this event computed as explained on this figure. As in the incident-shock test time results of Figs. 5 and 6, we see from Fig. 10 that (1) the air and nitrogen data are in good agreement (2) the data are in poor agreement with theory at high values of P_1 and in fair agreement at low values of P_1 and (3) the data exhibit substantially less sensitivity to P_1 than the theory would predict.

3.4 Data Analysis

In order to provide (1) a direct comparison of the radiation and end-wall pressure data in a way that takes into account differences in the axial location of the three instrumentation stations and (2) a convenient summary of the efficacy of Mirels' theory for various test conditions, the absolute test time and Δt "dip" results of Figs. 5, 6, and 10 are presented in Fig. 11 in terms of the ratio of the experimental to the theoretical time. Compared in this fashion, the end-wall pressure data, for a given P_1, consistently corroborates the radiation data. However, a residual effect of the driven-tube length over diameter ratio, Ls/d, seems to exist since the low Ls/d instrumentation station tends to be in better agreement with theory than the higher Ls/d station in any given run.* The general agreement with Mirels' theory therefore depends not only on the driven-tube initial pressure level P_1, as was pointed out earlier and is certainly apparent in Fig. 11, but also on the driven tube geometry involved in a particular experiment.**

*It should be remembered, in interpreting the data of Fig. 11, that the shock Mach number at the end-wall is about 0.5 Mach number units lower than the shock Mach number at station 5 in any given run (see Fig. 2).

**For shock-tube configurations and test conditions commonly used in high-pressure shock-tunnel work, the incident-shock test time and hence slug lengths are only about one half of that predicted by Mirels' theory.

Thorough analysis of the data of Figs. 5, 6, 10 and 11 has uncovered a possible explanation for these unexpected results. However, before pursuing this, it is desirable to first review some of the properties of the important viscous shock-tube parameters given by Mirels' theory.[1]

Mirels' equation for the viscous, incident-shock test time, τ, is given as

$$\frac{\tau}{\tau_i} = \left(\frac{1}{X}\right)\left(\frac{T}{1 + \frac{T^{4/5}}{W-1}}\right) \tag{1}$$

where W is the density ratio across the incident shock (i. e. $W \equiv \rho_2/\rho_1$) and τ_i is the inviscid, incident-shock test time given by the equation below in which a_1 represents the initial speed of sound of the driven gas.

$$\tau_i = \frac{L_s / a_1}{M_s (W-1)} \tag{2}$$

The viscous parameters X and T of Eq. 1 are defined by the following identities:

$$X \equiv \frac{\ell_i}{\ell_m} \tag{3}$$

$$T \equiv \frac{\ell}{\ell_m} \tag{4}$$

where ℓ_i is the inviscid-shock slug length (i. e. ℓ_i = Ls/W) and ℓ is the viscous incident-shock slug length. The variable ℓ_m represents the maximum possible separation distance between the incident shock and the contact surface which occurs when all the mass flow entering the shock, in a shock fixed coordinate system, is in the boundary layer and the contact surface moves at the same velocity as the shock front.

Mirels' shows that the parameter T is a function of the maximum separation distance parameter X according to the following implicit equation

$$X = -\frac{5}{4}\left(\ln \frac{1 - T^{1/5}}{1 + T^{1/5}} - 2\tan^{-1} T^{1/5} + 4 T^{1/5}\right) \tag{5}$$

From Equation 5 it can be shown that when $X \rightarrow \infty$, $T \rightarrow 1.0$ signifying that virtually all of the mass flow entering the shock is in the boundary layer. Conversely, when $X \rightarrow 0$, $T \rightarrow X$ indicating that very little of the mass flow entering the shock is in the boundary layer and hence the viscous slug length ℓ is very nearly equal to the inviscid slug length ℓ_i.

It is apparent from Eqs. 1 and 5 that the viscous over inviscid test time ratio, τ/τ_i depends simply on the maximum separation distance parameter X and the density ratio, W. Mirels' solves for the limiting slug length, ℓ_m, and therefore X by evaluating the mass flow in the boundary layer assuming a 1/7 power law for the velocity profile and an incompressible Blasius skin-friction law, applied to compressible flow by using Eckert's reference enthalpy technique for evaluating the fluid properties at a suitable temperature. Such analysis showed that ℓ_m was dependent on the driver tube diameter, d, and initial pressure P_1 according to the relation

$$\ell_m \sim p_1^{1/4} d^{5/4} \tag{6}$$

so from Eq. 3

$$X \sim \frac{L_s/d}{(p_1 d)^{1/4}} \tag{7}$$

Solutions for Mirels' maximum separation distance parameter, X, for air and nitrogen are presented in Fig. 12* in the normalized form

*These results, obtained from the computer program referred to earlier, are based on the following numerical constants evaluated at an initial gas temperature, T_1, of 75°F which closely approximates the actual experimental test condition. $p_{st} = 1$ atm

Driven Gas	Specific heat ratio γ_1	a_1 ft/sec	Sutherland constant °K	Viscosity, lb_f-sec/ft^2 μ_1	Prandtl No.	$\frac{\gamma_1 p_{st}}{a_1 \mu_1}$ ft^{-1}
N_2	1.4	1152.87	104	3.7015×10^{-7}	0.713	6.942×10^6
Air	1.4	1133.79	110.4	3.8262×10^{-7}	0.709	6.829×10^6

suggested by Eq. 7. It is apparent from this figure that the maximum separation distance parameter, X, is a comparatively weak function of shock Mach number, M_s, and initial pressure, P_1, particularly in the range of M_s and P_1 covered in these experiments. The parameter X, therefore is determined almost exclusively by the normalizing parameter $(P_1 d)^{1/4} / (Ls/d)$. As a result, τ/τ_i is similarly dependent on this parameter as can be seen by rewriting Eq. 1 in the form below

$$\frac{\tau}{\tau_i} = (C_1)\left[\frac{(p_1 d)^{1/4}}{L_s/d}\right]\left(\frac{T}{1+\frac{T^{4/5}}{W-1}}\right) \qquad (8)$$

where $$C_1 = \left[\frac{(X)(p_1 d)^{1/4}}{L_s/d}\right]^{-1} \simeq \text{constant (see Fig. 12).} \qquad (9)$$

It is of interest now to present the data of Figs. 5, 6, and 10 in the form suggested by Eq. 8 in order to evaluate the functional behavior of the data relative to the theory. This result is given in Fig. 13 which clearly demonstrates that the data can not be correlated by the parameter $(Ls/d) / (P_1 d)^{1/4}$ predicted by Mirels' theory. However, unlike previous presentations (i.e. Fig. 5, 6, 10, and 11) the data does possess a definite coherency when viewed in this fashion for now the data organizes itself in three levels of the viscous over inviscid time ratio which are essentially independent of P_1 and vary linearly with the Ls/d of the corresponding instrumentation station. This observation suggested the correlation of data presented in Fig. 14 which proved very successful and provides insight into the probable reason that Mirels' theory fails to adequately predict incident-shock test time. The fact that the data correlate in the manner given in Fig. 14 strongly suggests that the mass flow in the boundary layer is much greater than is taken into account in Mirels' theory. The basis for this conjecture is given in the discussion that follows.

If we assume that for these test conditions <u>all</u> rather than only a portion of the mass flow entering the shock is in the boundary layer, then T by definition of 1.0 and Eq. 8 reduces to the following form

$$\left(\frac{\tau}{\tau_i}\right)\left(\frac{L_s}{d}\right) = (C_1)(p_1 d)^{1/4}\left(1 - \frac{1}{W}\right) \qquad (10)$$

But now the exponent of the (P_1 d) term must be less than 1/4 since when the theoretical mass flow in the boundary layer is made to increase at a given station, as a result of changes in the assumed velocity profile and skin friction law, the exponent of the (P_1 d) term will decrease. This can be seen by comparing the functional behavior of ℓ_m for a laminar boundary which is a low mass-flow sink to that of a turbulent boundary layer which is a relatively high mass-flow sink. Mirels shows in Ref. 1 that regardless of whether the boundary layer is laminar or turbulent ℓ_m may be expressed as

$$\ell_m \sim (d)(p_1 d)^{\frac{n}{1-n}} \tag{11}$$

For a laminar boundary layer, n = 1/2 and for the turbulent boundary layer assumed by Mirels in Ref. 1, n = 1/5 so

$$\ell_m \sim (d)(p_1 d) \quad , \text{ LAMINAR} , \quad n = 1/2 \tag{12}$$

$$\ell_m \sim (d)(p_1 d)^{1/4} \quad , \text{ TURBULENT} , \quad n = 1/5 \tag{13}$$

The reduction in the exponent of the (P_1 d) term as the mass flow in the boundary layer increases from the laminar to the turbulent case is clearly demonstrated by these last two equations (i.e. Eq. 12, 13).

Using the general expression of Eq. 11 in Eq. 10 then gives

$$\left(\frac{\tau}{\tau_i}\right)\left(\frac{L_s}{d}\right) = (C_2)(p_1 d)^{\frac{n}{1-n}} \left(1 - \frac{1}{W}\right) \tag{14}$$

where $n < 1/5$ and

$$C_2 = \left[\frac{(X)(p_1 d)^{\frac{n}{1-n}}}{L_s/d}\right]^{-1} \approx \text{CONSTANT} \tag{15}$$

If n were of the order of 1/10 to 1/20, which is likely since little or no sensitivity to P_1 can be detected in the test-time data of Figs. 5, 6 and 10 then the parameter (τ/τ_i) (Ls/d) of Eq. 14 would be essentially constant for the range of test conditions covered in these experiments.

Within experimental accuracy, the data correlated as shown in Fig. 14 is seen to behave exactly as would be theoretically expected from Eq. 14. Since the Eq. 14 was derived assuming that the mass flow in the boundary layer was greater than predicted by Mirels' theory and that the limiting slug-length condition was achieved, the results of Fig. 14 not only suggests that the theory underestimates the boundary-layer mass flow but also that limiting slug lengths occur at much higher values of P_1 and lower values of Ls/d than was formerly believed.

In view of these results it appears that, although Mirels' theory is conceptually correct, the 1/7 power-law velocity profile and the incompressible Blasius skin-friction law used in developing that theory inadequately describes the high Reynolds number (i. e. $Re > 10^7$), high Mach number type flows to which this theory is frequently applied. Better agreement with experimental data might therefore be obtained by modifying Mirels' theory such that the solution of the shock-tube momentum integral equation is based on (1) the apparently universal velocity profile defined by Coles [27] well-known "Law of the Wall-Law of the Wake" equation and (2) a compressible skin-friction formula such as given by Nash and Macdonald [28].

4. CONCLUSIONS

Measurements of incident-shock test time and end-wall reflected-shock pressure have been presented for fully turbulent boundary-layer test conditions at shock Mach numbers ranging from 7.5 to 10.6 in air and nitrogen. Incident-shock test time and hence reflected-shock slug lengths were found to be considerably less than Mirels' theory predicts at the test conditions commonly used in high-pressure shock-tunnel work. Little or no sensitivity to P_1 could be detected in the experimental test-time data. The ratio of the experimental time to the inviscid time (i.e., τ/τ_i) multiplied by the Ls/d of the instrumentation station proved to be essentially constant for the range of test conditions reported herein. This is contrary to Mirels' theory which predicts a nonlinear dependence of τ/τ_i on the parameter $(P_1 d)^{1/4} / (Ls/d)$. Such results suggest that limiting slug lengths and hence maximum incident-shock test times probably occur at much higher values of P_1 and lower values of Ls/d than was formerly believed.

Comparison of the air and nitrogen data showed conclusively that combustion between the driver and driven gas, when hydrogen and air gas combinations are employed, is not responsible for the discrepancy in incident-shock test time observed. Combustion appears to occur in a region of mixed driver and driven gas that always exists behind the incident shock and for this reason combustion does not consume usable test gas. The end-wall pressure measurements, which provided an independent check both on the existence of a combustion region and on the location of the interface region near the end of the driven tube, consistently corroborated the radiation measurements for both air and nitrogen.

Measurements of shock-tube boundary-layer transition time showed that the test conditions of these experiments closely approximated Mirels' requirement that the boundary-layer behind the incident shock be fully turbulent. These data, which were obtained at a unit Reynolds number believed to be higher than has ever been reported in the open literature for high-wall cooling rates (i.e. $M_s \approx 8$), are in fairly good agreement with

the transition Reynolds-number correlation of Hartunian, et al. [21]

The apparent reason for the discrepancy between the experimental and theoretical incident-shock test times is that the mass flow in the boundary layer is greater than Mirels' theory would predict. The problem probably stems from using a 1/7 power law for the velocity profile and an incompressible skin-friction law in developing this theory. However, definite proof of this conjecture awaits solutions based on a more reliable velocity profile such as defined by Coles [27] and a compressible skin-friction law such as given by Nash and Macdonad [28].

REFERENCES

1. Mirels, H.: "Shock Tube Test Time Limitations Due to Turbulent Wall Boundary Layer," Aerospace Rept. No. TDR-169 (3230-12) TR-3, May 6, 1963; also AIAA Journal, Vol. 2, No. 1, Jan., 1964, pp. 84-93.

2. Mirels, H.: "Test Time in Low-Pressure Shock Tubes," Aerospace Report No. TDR-169 (3230-12) TN-5, Dec. 27, 1962; also The Physics of Fluids, Vol. 6, No. 9, Sept., 1963, pp. 1201-1214.

3. Brocher, E. F.: "Hot Flow Length and Testing Time in Real Shock Tube Flow," The Physics of Fluids, Vol. 7, No. 3, March, 1964, pp. 347-351.

4. Bertin, J. J.: "Analysis of Test Times and Boundary Layer Induced Property Variations in a Circular Shock Tube," NASA TN D-3759, Jan., 1967.

5. Roshko, A.: "On Flow Duration in Low Pressure Shock Tubes," The Physics of Fluids, Vol. 3, No. 6, Nov.-Dec., 1960, pp. 835-842.

6. Hooker, W. J.: "Testing Time and Contact-Zone Phenomena in Shock-Tube Flows," The Physics of Fluids, Vol. 4, No. 12, Dec., 1961, pp. 1451-1463.

7. Ackroyd, J. A. D.: "A Study of Running Times in Shock Tubes," Aeronautical Research Council Rept. C. P. No. 722, July, 1963.

8. Camm, J. C. and Rose, P. H.: "Electric Shock Tube for High Velocity Simulation," Avco-Everett Research Laboratory, Research Report 136, July, 1962.

9. Duff, R. E.: "Shock Tube Performance at Low Initial Pressure," The Physics of Fluids, Vol. 2, No. 2, March-April, 1959, pp. 207-216.

10. Sandborn, V. A.: "Measurements of Flow Duration in a Low-Pressure Shock Tube," NASA TN D-1218, May, 1962.

11. Sandborn, V. A., Weisblatt, H., and Flagg, R. F.: "Test Time in a 1.5-Inch Diameter High-Stagnation-Enthalpy Shock Tube," AIAA Journal, Vol. 1, No. 5, May, 1963, pp. 1236-1237.

12. Graber, B. C. and Nerem, R. M.: "Test Duration Measurements in an Arc-Driver Hypervelocity Shock Tube," The Ohio State University Research Foundation Rept. No. 1573-2, October 15, 1963.

13. Chaplin, S. G. and Rumpel, W. F.: "Measurements of Uniform Flow Duration in a Chambered, Buffered Shock Tube," AIAA Journal Tech. Notes Vol. 2, No. 8, August, 1964, pp. 1499-1500.

14. Dunn, M. G.: "Experimental Shock-Tube Investigations of Conditions Behind Incident and Reflected Shocks in Air for Shock Mach Numbers Between 8.5 and 16.5," CAL Report No. AI-2187-A-3, October, 1966; also Fifth Hypervelocity Techniques Symposium, Denver, Colorado, March, 1967.

15. Livingston, F. R.: "Experimentally Measured Effects of the Wall Boundary Layer on Shock-Tube Peformance," Jet Propulsion Laboratory Tech. Report No. 32-714, March 1, 1965.

16. Roshko, A. and Smith, J. A.: "Measurements of Test Time in the GALCIT 17-Inch Shock Tube," AIAA Journal, Vol. 2, No. 1, Jan., 1964, pp. 186-187.

17. Appleton, J. P. and Musgrove, P. J.: "An Investigation of the Departure from Ideal Shock Tube Performance. Preliminary Results," Dept. of Aeronautics and Astronautics, University of Southampton, April, 1963.

18. Bird, K. D., Martin, J. F. and Bell, T. J.: "Recent Developments in the Use of the Hypersonic Shock Tunnel as a Research and Development Facility," Third Hypervelocity Symposium, Denver, Colorado, 1964.

19. Hilsenrath, J., Beckett, C. W., Benedict, W. S. et al.: "Tables of Thermal Properties of Gases," National Bureau of Standards Circular 564, November 1, 1955.

20. Vidal, R. J.: "Model Instrumentation Techniques for Heat Transfer and Force Measurements in a Hypersonic Shock Tunnel," Cornell Aeronautical Laboratory Rept. AD-917-A-1, February, 1956.

21. Hartunian, R. A., Russo, A. L. and Marrone, P. V.: "Boundary-Layer Transition and Heat Transfer in Shock Tubes," Cornell Aeronautical Laboratory Rept. AD-1118-A-3, December, 1959.

22. Kurzrock, J. W.: "Selection of Surface Thermometers for Measuring Heat Flux," Cornell Aeronautical Laboratory Rept. No. 124, February, 196.

23. Flagg, R. F.: "Advances in Shock Tunnel Driving Techniques," Third Hypervelocity Techniques Symposium, Denver, Colorado, 1964, pp. 89-115.

24. Lewis, C. H. and Burgess. E. G.: "Charts of Normal Shock Wave Properties in Imperfect Air [Supplement: M_S = 1 to 10]"AEDC-TR-65-196, Sept., 1965; also Numerical Tabulations of Air Normal Shock Properties provided by private communications with C. H. Lewis.

25. Lewis, C. H. and Burgess, E. G.: "Charts of Normal Shock Wave Properties in Imperfect Nitrogen [Supplement: M_S = 1 to 10]" AEDC-TR-66-116, September, 1966; also Numerical Tabulations of Nitrogen Normal Shock Properties provided by private communications with C. H. Lewis.

26. Dunn, M. G.: "Experimental Study of Reflected-Shock Tunnel Flows in the Equilibrium Interface Region," Cornell Aeronautical Laboratory Rept. No. AM-1702-A-1, January, 1968.

27. Coles, Donald: "The Law of the Wake in the Turbulent Boundary Layer," Journal of Fluid Mechanics, Vol. 1, Part 2, p. 191, July 1956.

28. Nash, J. F. and Macdonald, A. G. J.: "A Turbulent Skin-Friction Law for Use at Subsonic and Transonic Speeds," National Physical Laboratory, England NPL Aero Report 1206, A. R. C. 28 234, July 29, 1966.

29. Lacey, J. J.: "Experimental Shock Tube Test Time-Turbulent Regime," AEDC-TR-69-131, August, 1969.

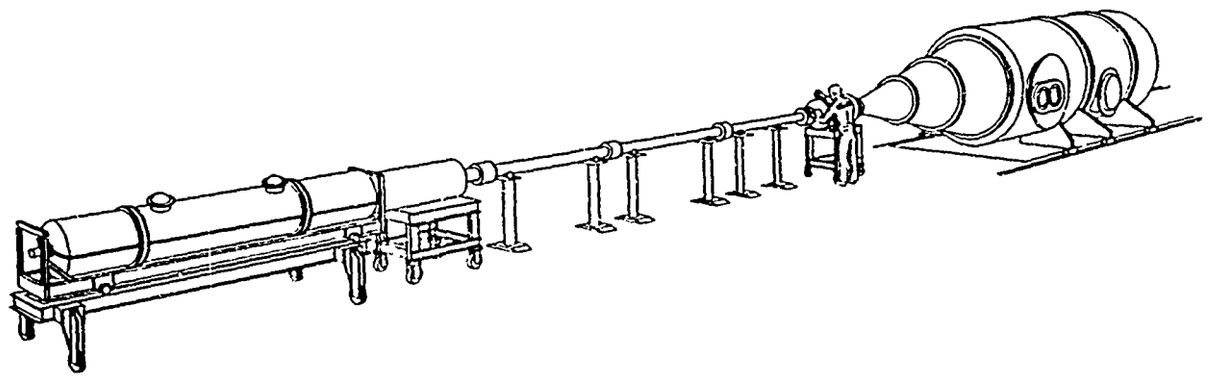

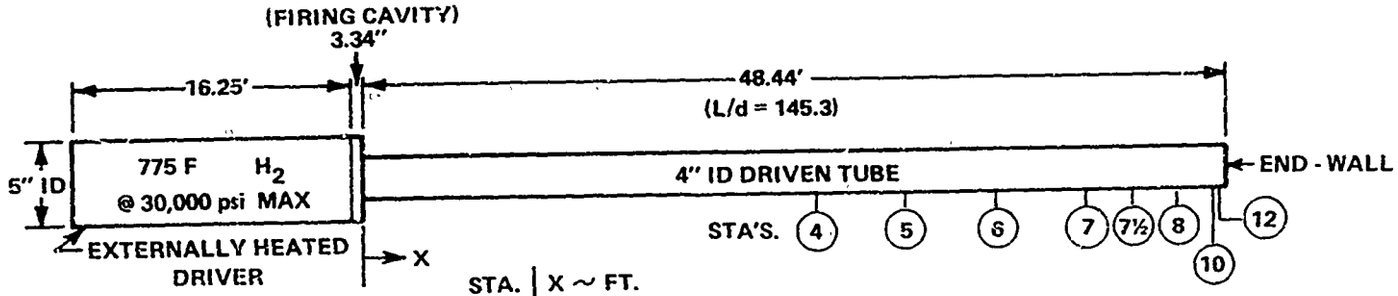

STA.	X ~ FT.
4	25.67
5	30.67
6	35.67
7	40.67
7-1/2	43.17
8	45.67
10	47.87
12	48.37

Figure 1 BASIC COMPONENTS OF THE CAL HYPERSONIC SHOCK TUNNEL 96" HIGH ENERGY LEG

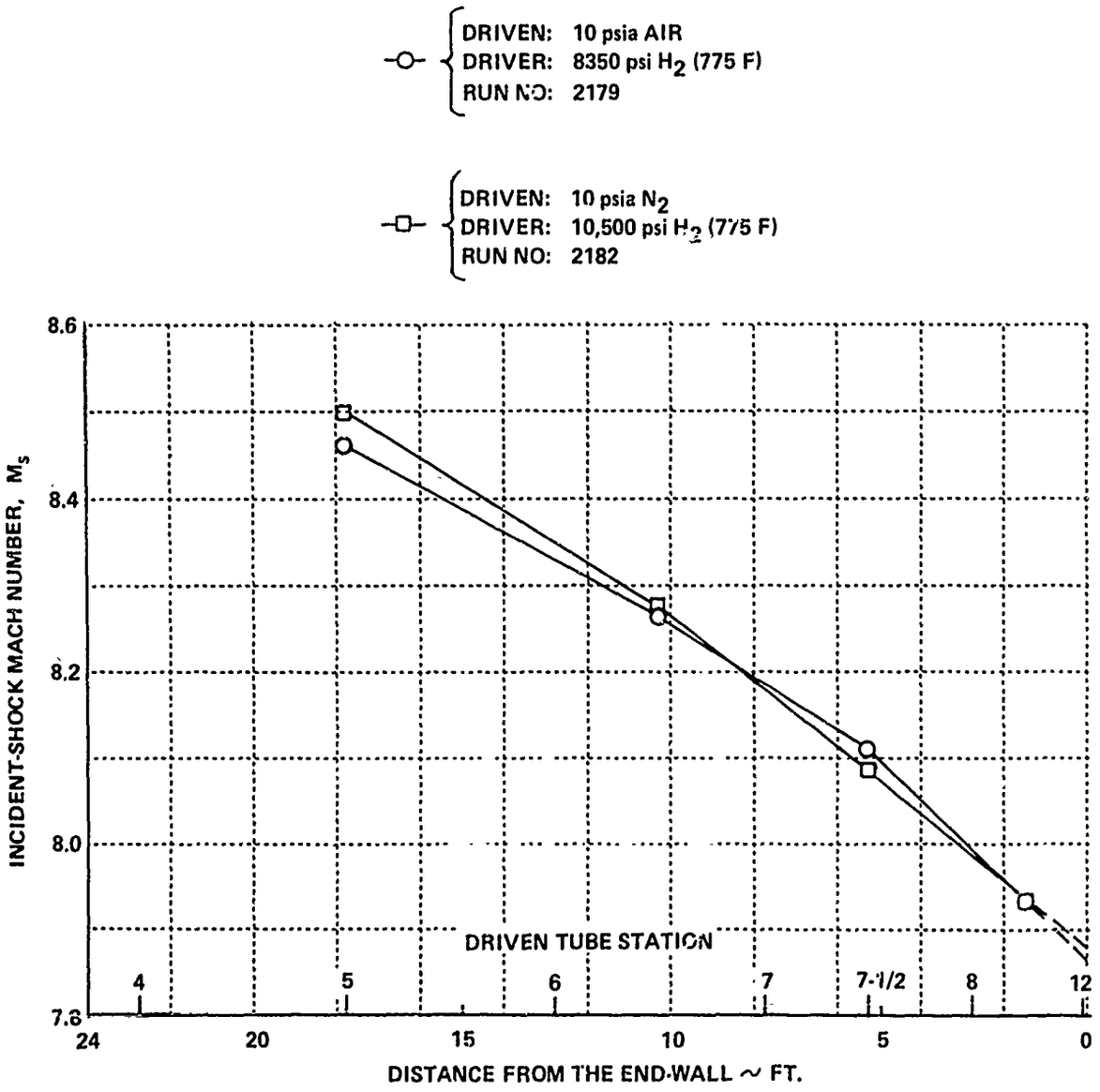

Figure 2 TYPICAL ATTENUATION CHARACTERISTICS OF THE INCIDENT SHOCK

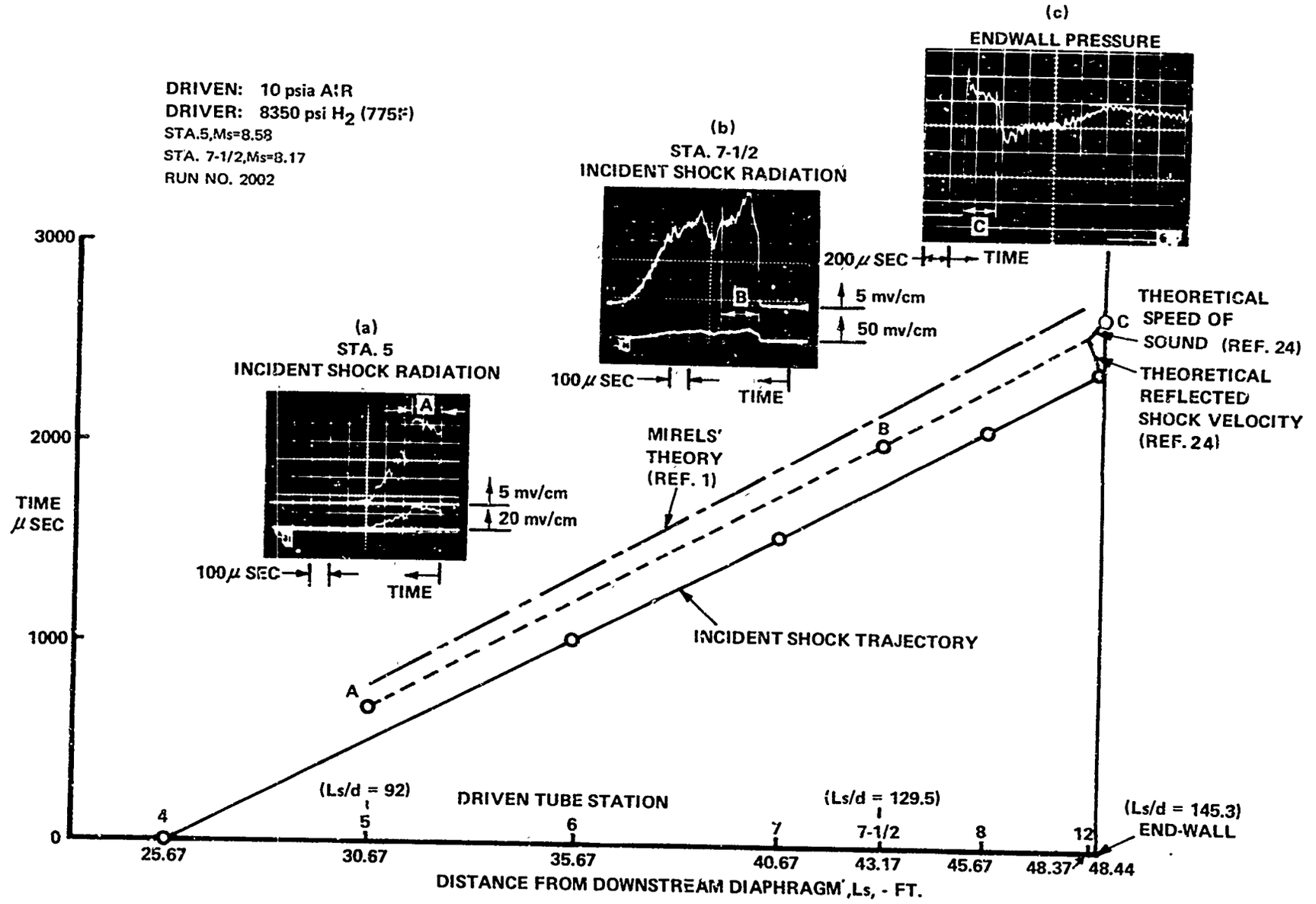

Figure 3 WAVE DIAGRAM CONSTRUCTED FROM EXPERIMENTAL DATA

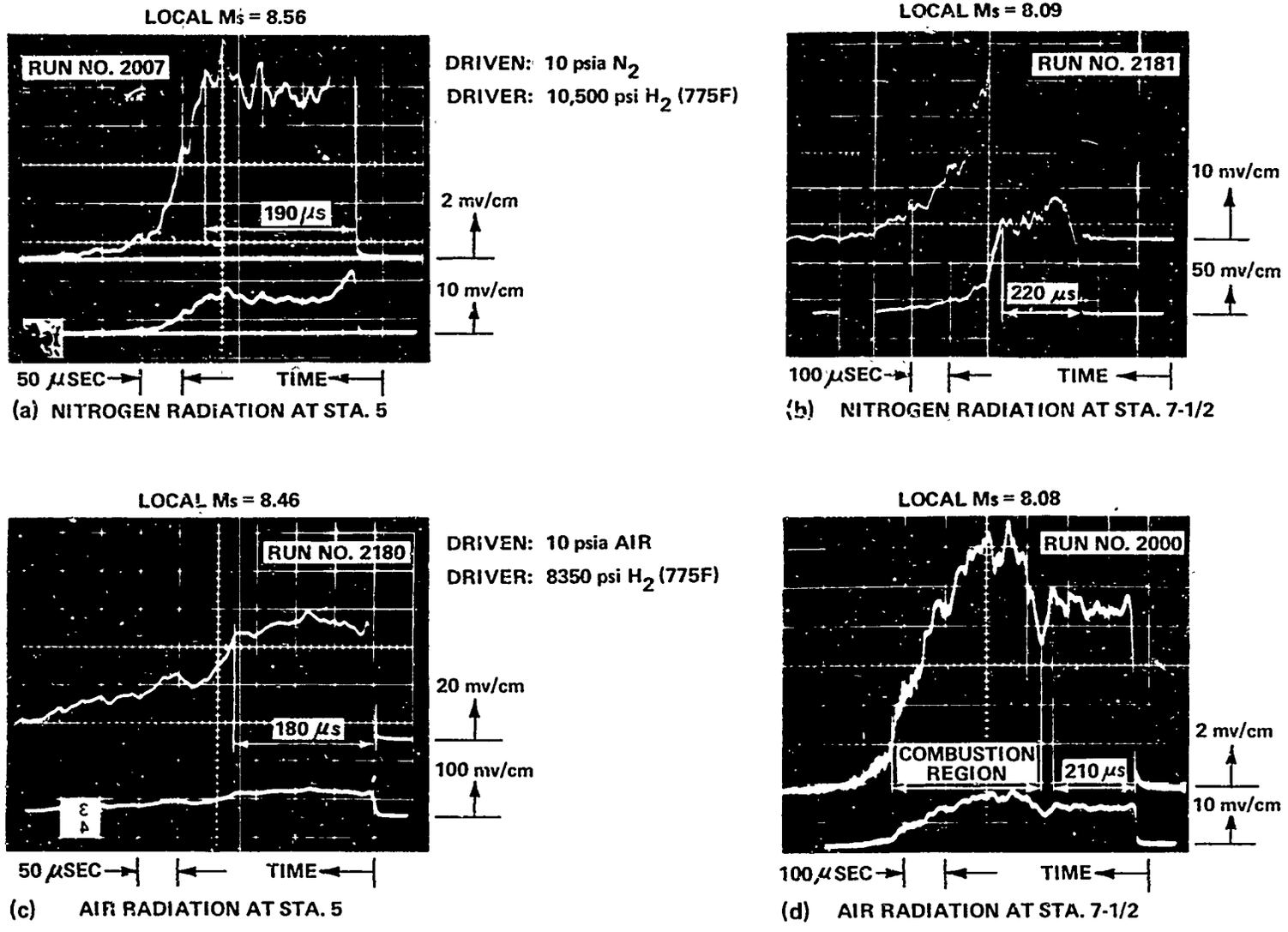

Figure 4 INCIDENT SHOCK RADIATION FOR NITROGEN AND AIR

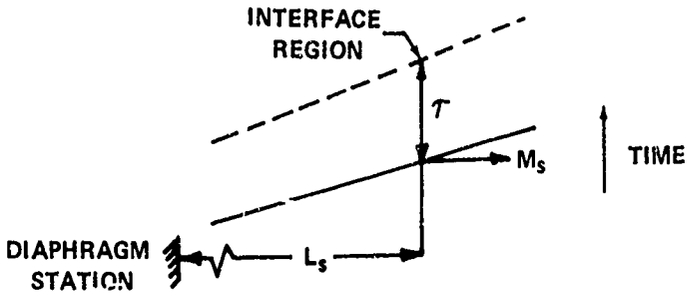

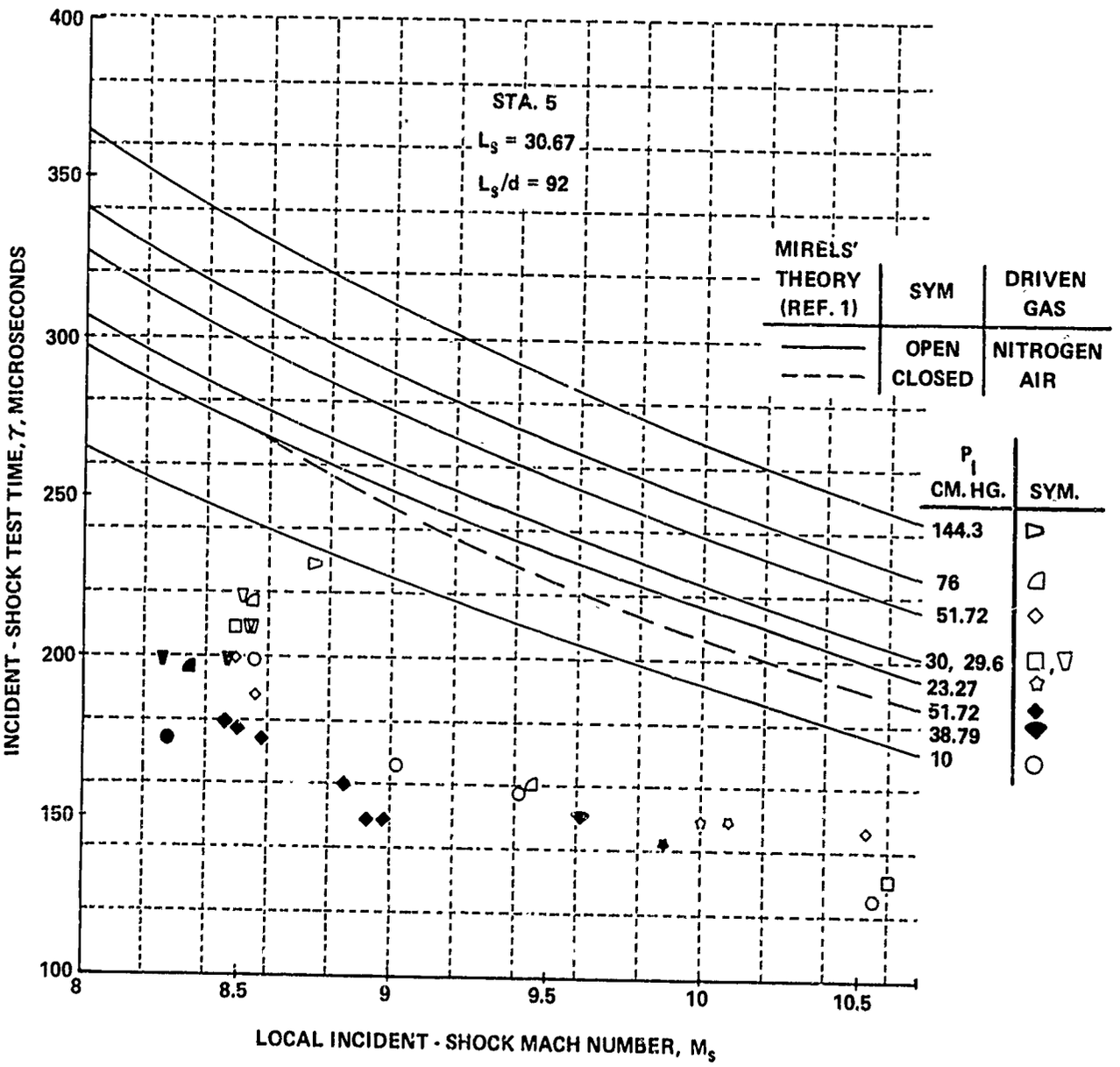

Figure 5 INCIDENT - SHOCK TEST TIME AT STA. 5

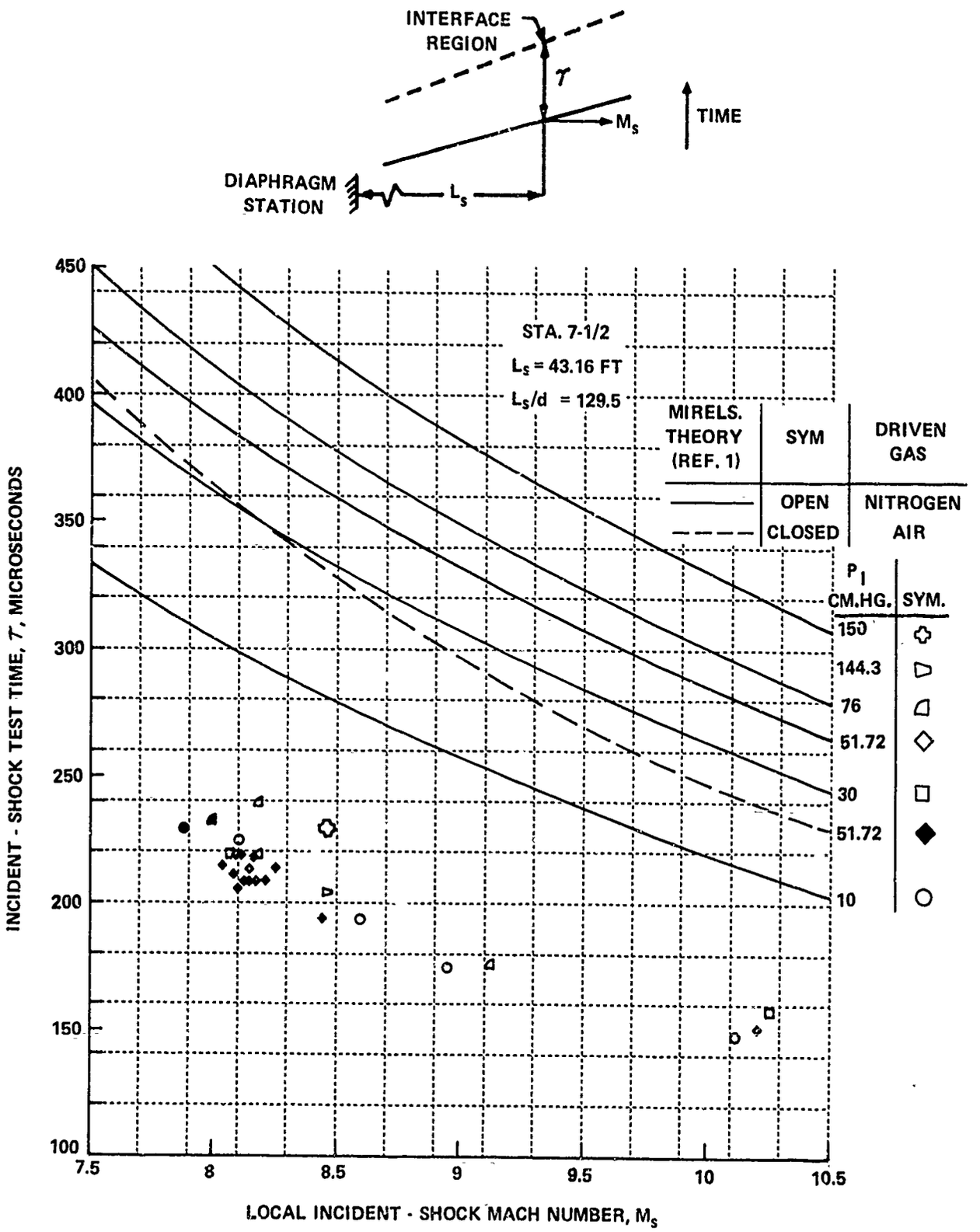

Figure 6 INCIDENT - SHOCK TEST TIME AT STA. 7-1/2

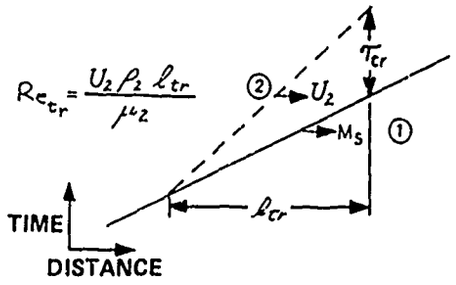

AIR
P_1 = 10 psia
STA 10

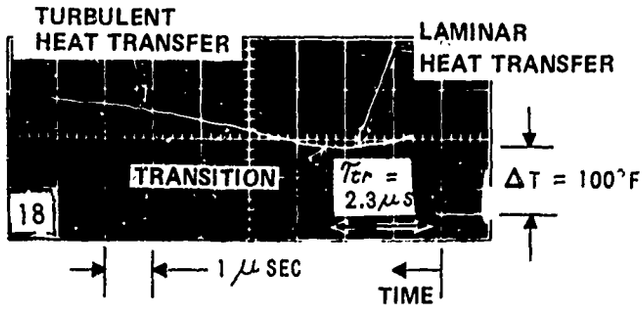

DRIVER: 8350 psi H_2 (775F)
LOCAL M_s = 7.86
Re/FT = 53 x 10^6
Re_{tr} = 6.76 x 10^6
RUN NO. 2180

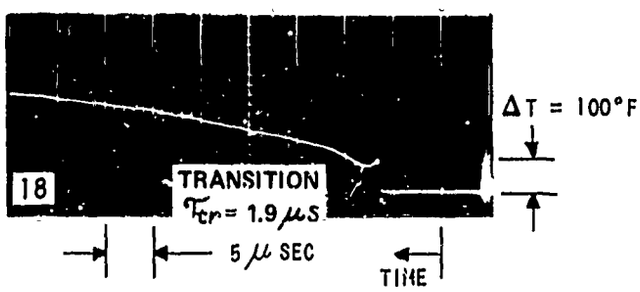

DRIVER: 8200 psi H_2 (775F)
LOCAL M_s = 7.97
Re/FT = 53.6 x 10^6
Re_{tr} = 5.76 x 10^6
RUN NO. 2177

Figure 7 TYPICAL WALL - TEMPERATURE RECORDS SHOWING BOUNDARY - LAYER TRANSITION

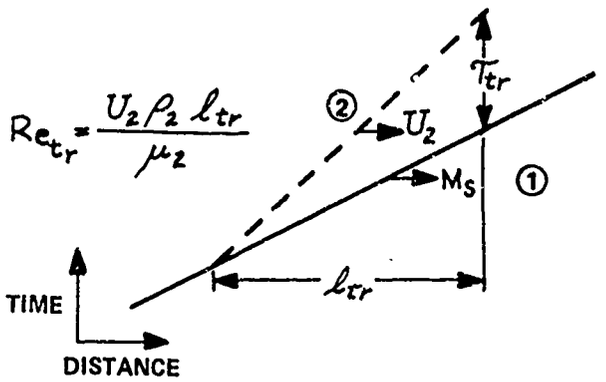

SYM	DRIVEN GAS	P_1 cm. Hg	M_s	UNIT REYNOLDS NUMBER Re/FT x 10^{-6}	τ_{tr} μ SEC
●	AIR	51.72	7.9	53	1.4 - 3.4
○	N_2	↓	7.96	48.6	2.5
■	AIR	10	7.6	10	1.6
□	N_2	↓	8.7	9.7	1.2

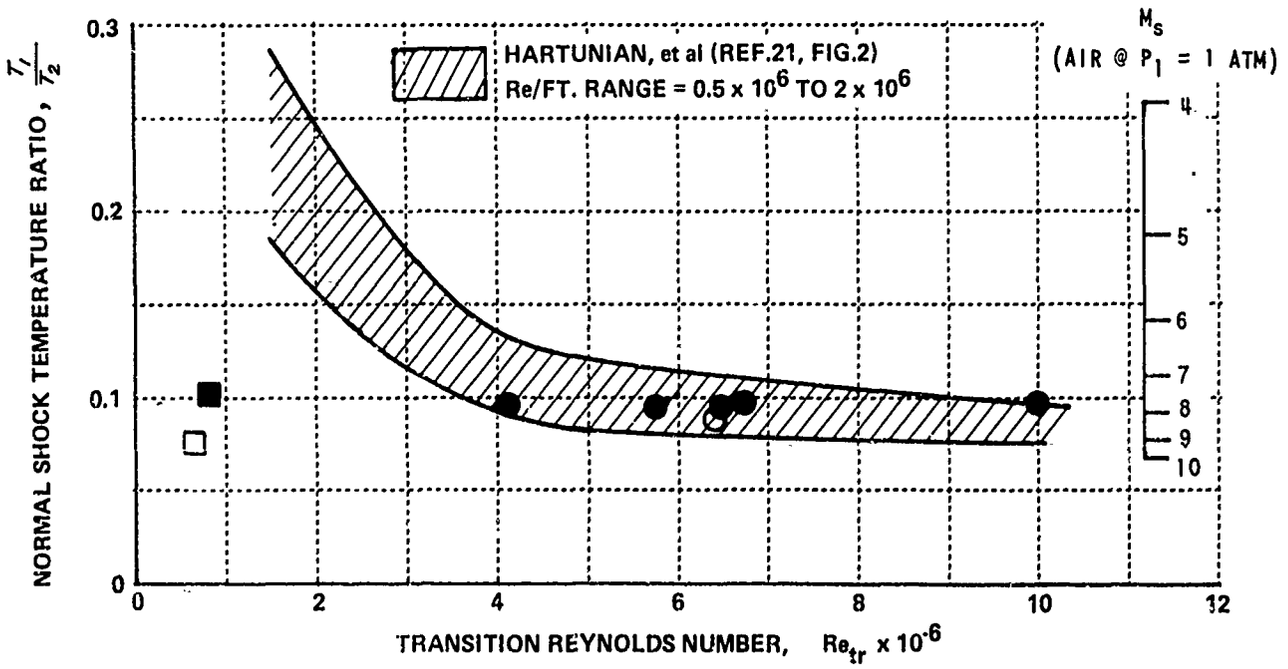

Figure 8 SHOCK-TUBE BOUNDARY-LAYER TRANSITION REYNOLDS NUMBER

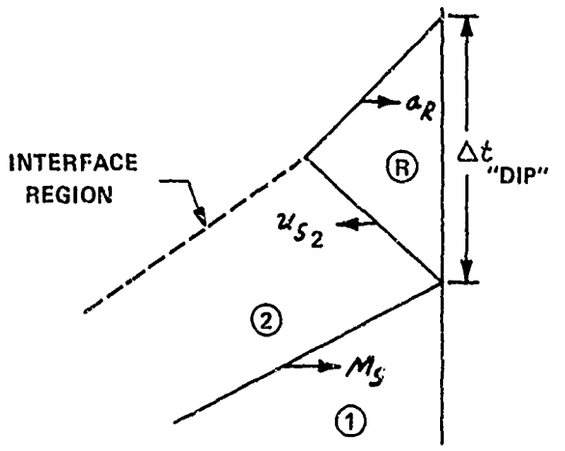

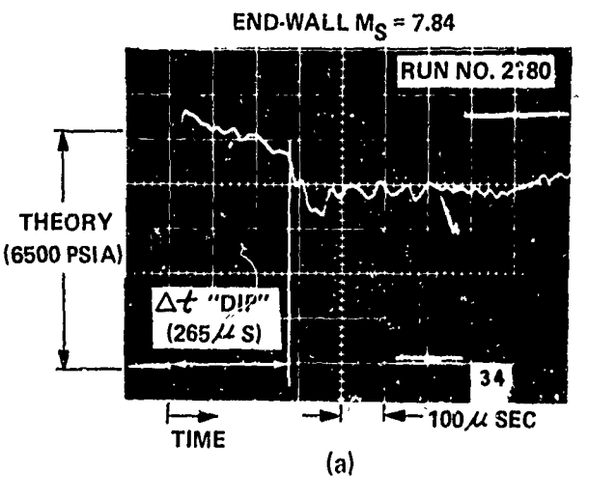

DRIVEN: 10 psia AIR
DRIVER: 8350 psi H_2 (775F)

(a)

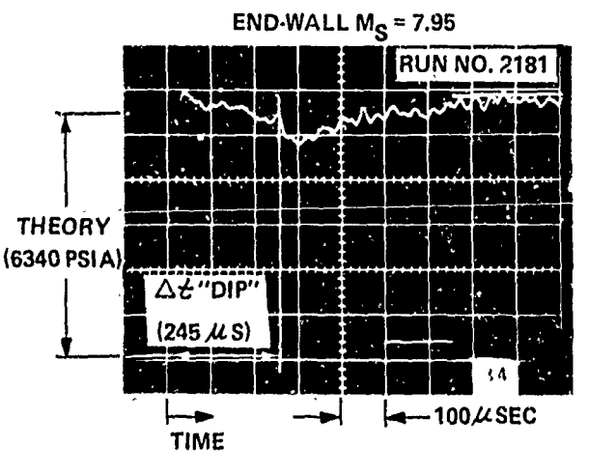

DRIVEN: 10 psia N_2
DRIVER: 10,500 psi H_2 (775F)

(b)

Figure 9 END-WALL REFLECTED - SHOCK PRESSURE

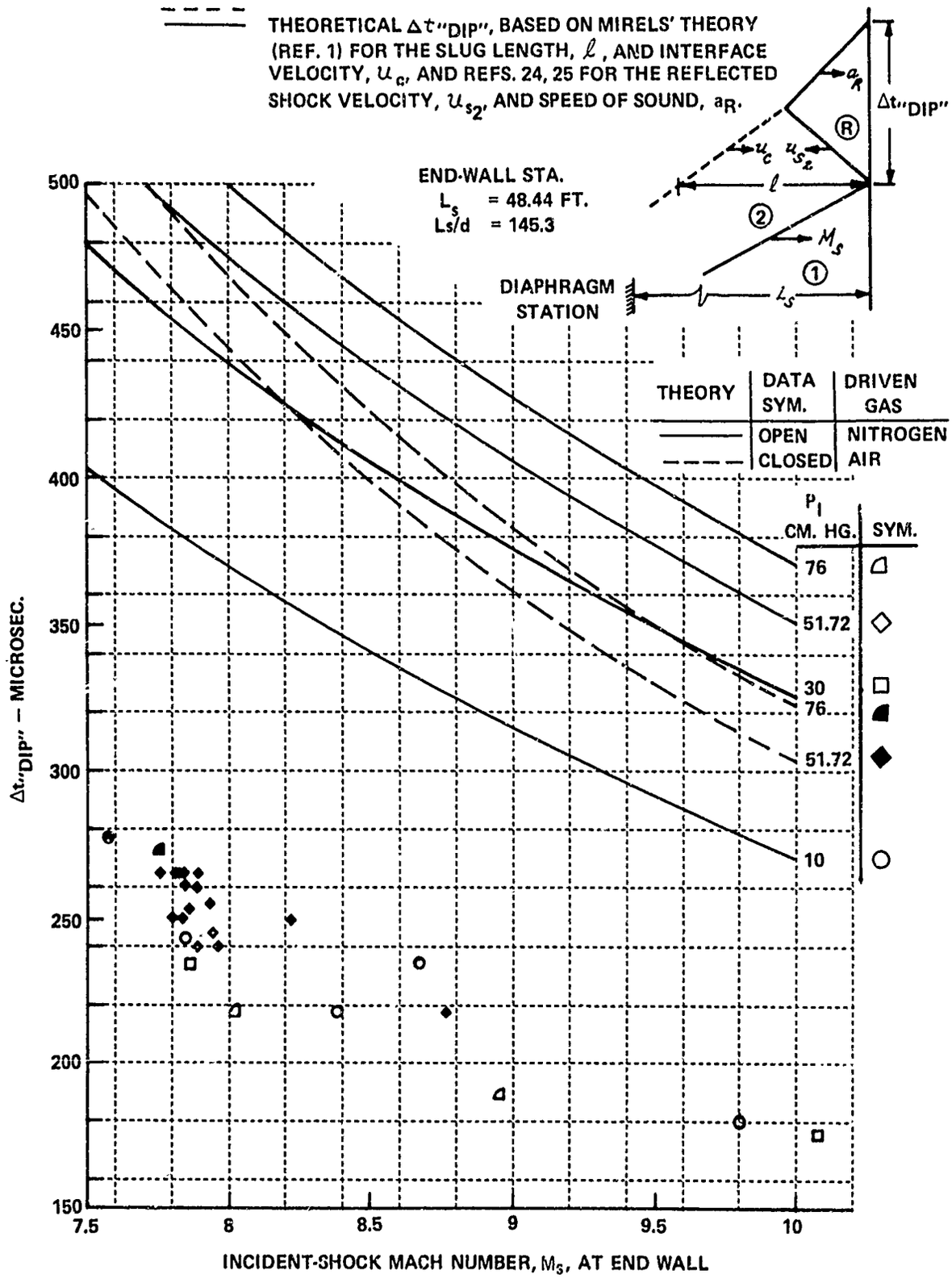

Figure 10 COMPARISON OF EXPERIMENTAL AND THEORETICAL TIME FOR THE "DIP" IN END WALL PRESSURE

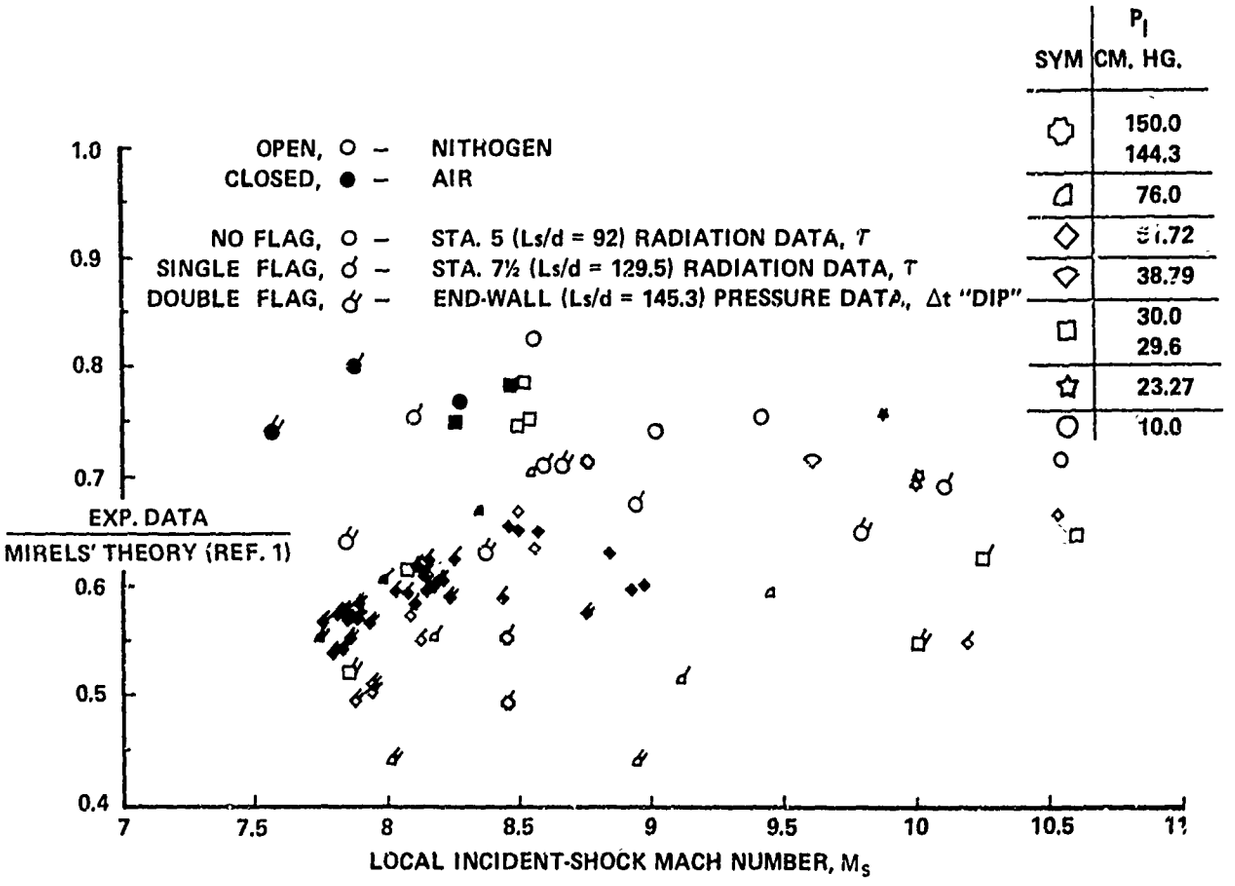

Figure 11 RATIO OF EXPERIMENTAL DATA TO MIRELS' THEORETICAL INCIDENT-SHOCK TEST TIME, τ, AND END-WALL Δt "DIP"

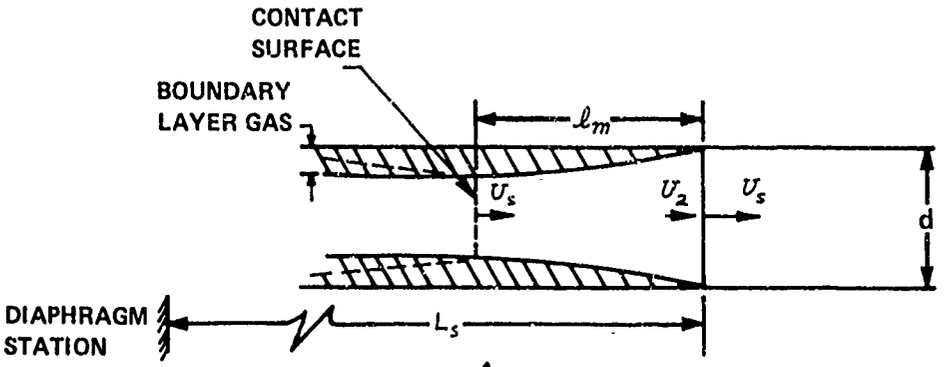

$$X = \frac{\ell_i}{\ell_m}$$

where

ℓ_i = INVISCID SEPARATION DISTANCE
ℓ_m = MAXIMUM SEPARATION DISTANCE

——— BASED ON REAL GAS NORMAL SHOCK PROPERTIES OF REFS. 24, 25
– – – – – BASED ON IDEAL GAS NORMAL SHOCK PROPERTIES

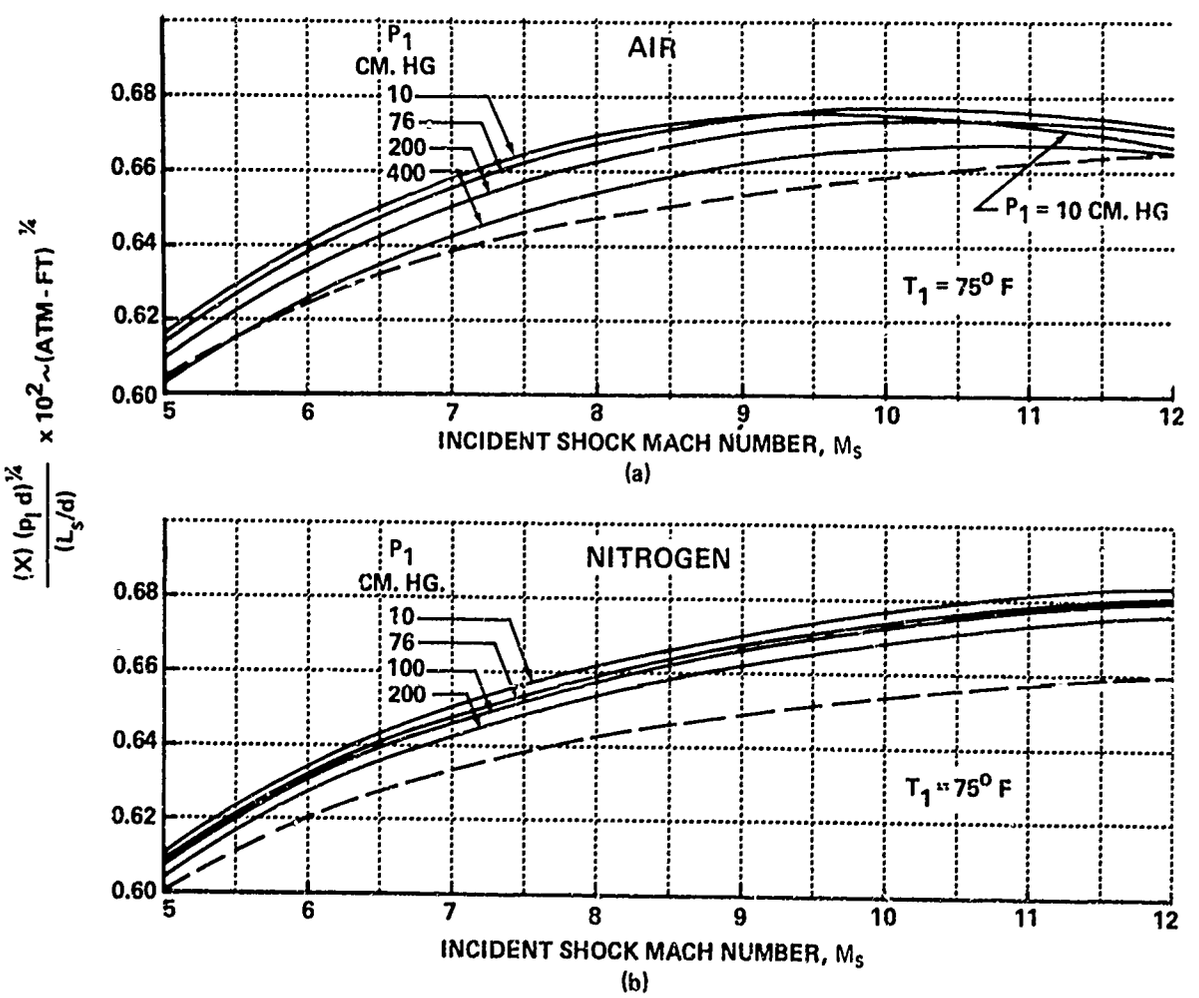

Figure 12 NORMALIZED FORM OF MIRELS' MAXIMUM SEPARATION DISTANCE PARAMETER, X, (REF. 1)

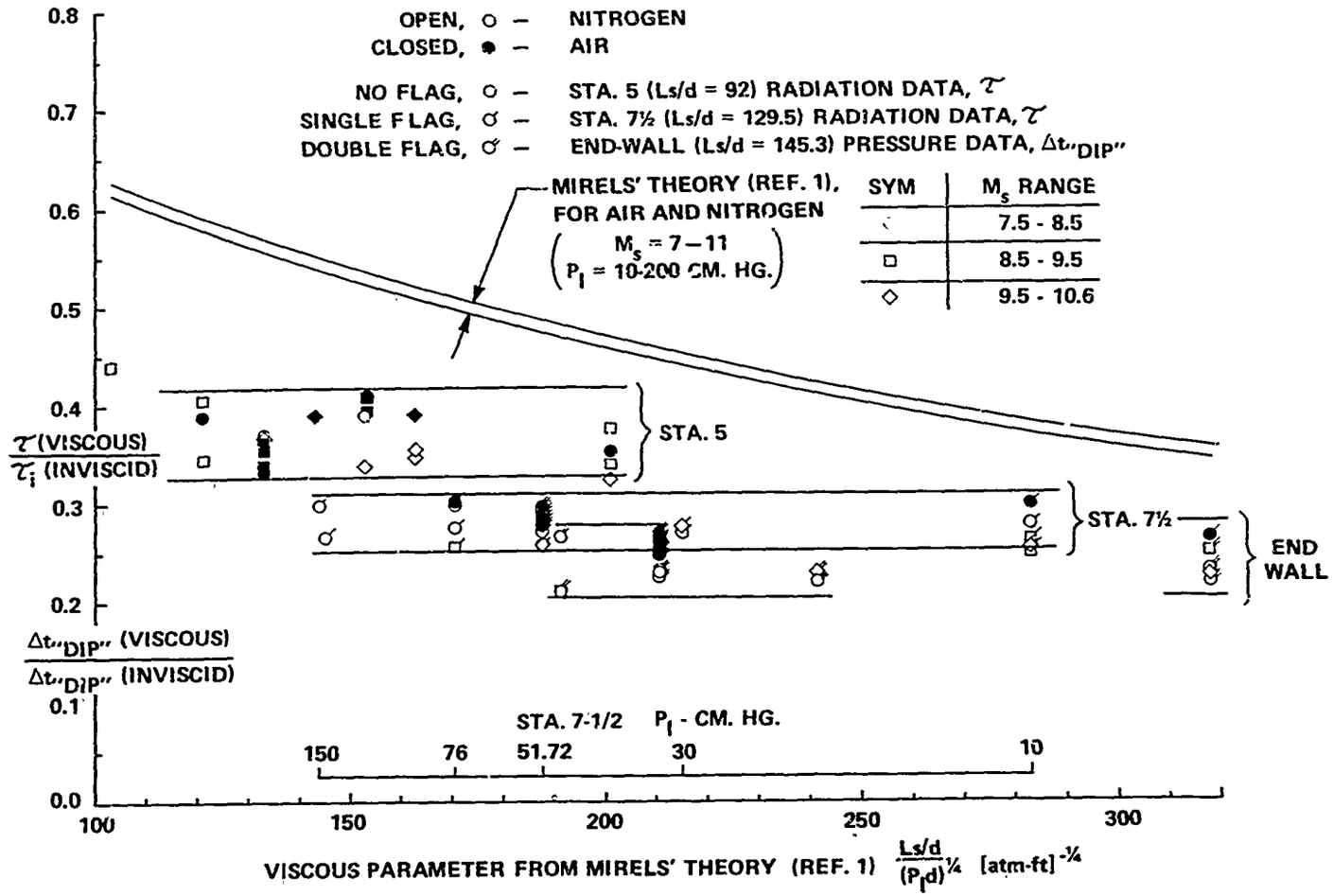

Figure 13 RATIO OF VISCOUS TO INVISCID INCIDENT-SHOCK TEST TIME AND Δt"DIP"

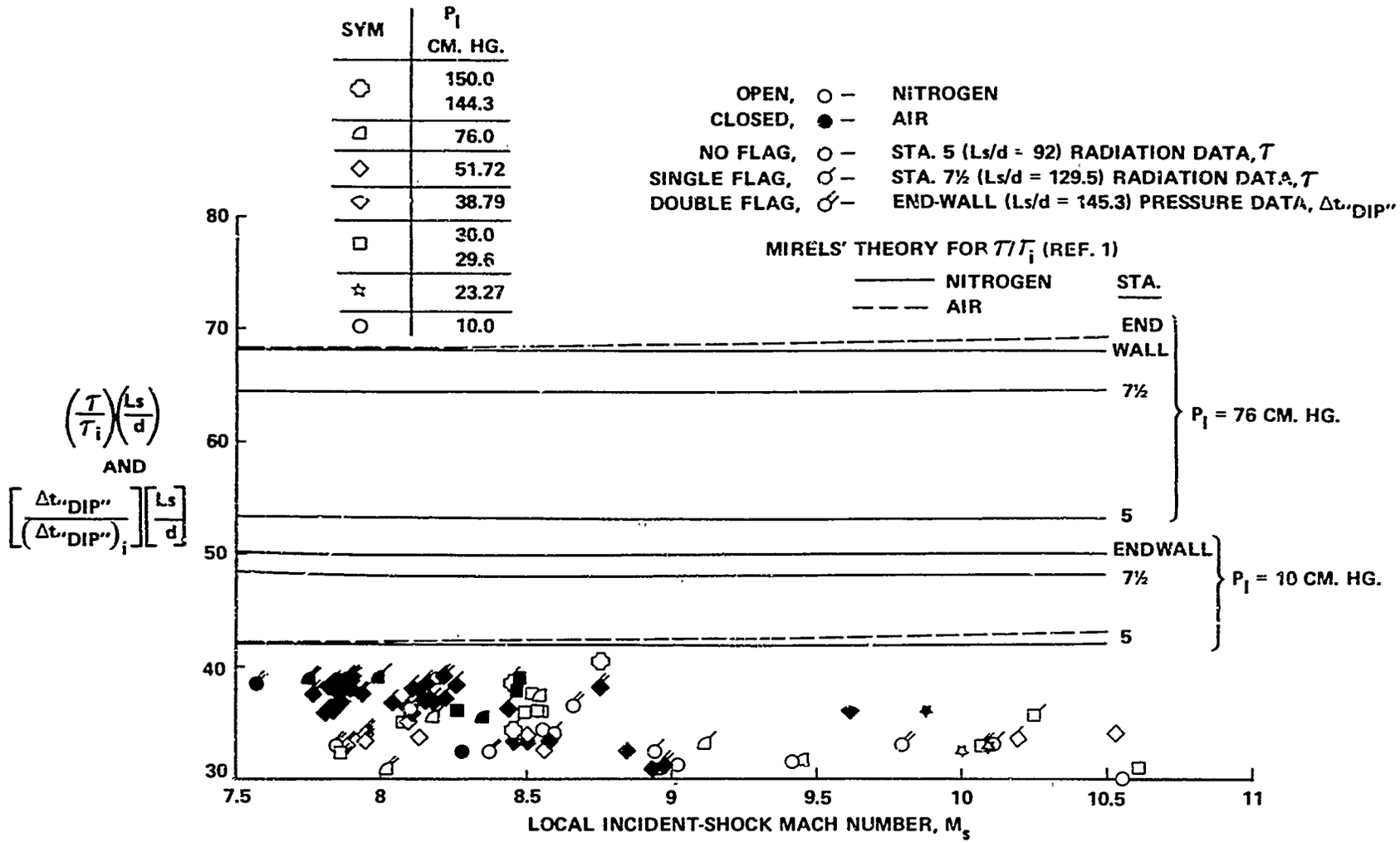

Figure 14 CORRELATION OF INCIDENT-SHOCK TEST TIME FOR TURBULENT BOUNDARY LAYER AND LARGE Ls/d TEST CONDITIONS